Dynamic Modeling with Experimental Calibration for the Syngas Production from Biomass Fixed-bed Gasification

Xin He [1+], Qiang Hu [1+], Haiping Yang[2], Christine Annette Shoemaker[3*], Chi-Hwa Wang [4*]

[1] *Energy and Environmental Sustainability Solutions for Megacities (E2S2), Campus for Research Excellence and Technological Enterprise (CREATE), Singapore 138602, Singapore*

[2] *State Key Laboratory of Coal Combustion, School of Energy and Power Engineering, Huazhong University of Science and Technology*

[3] *Department of Industrial Systems Engineering & Management, National University of Singapore, 1 Engineering Drive 2, Singapore 119260*

[4] *Department of Chemical and Biomolecular Engineering, National University of Singapore, 4 Engineering Drive 4, Singapore 117585*

*Corresponding Addresses: shoemaker@nus.edu.sg (Christine Annette Shoemaker)

chewch@nus.edu.sg (Chi-Hwa Wang)

+ Equal contribution authors

Abstract

In this paper, a dynamic biomass gasification model was developed based on the hybrid peripheral fragmentation and shrinking-core (HPFS) model. To improve the accuracy of syngas generation transient prediction, the chemical kinetic model was trained using global surrogate optimization techniques. The pre-exponential factors of kinetic reactions are calibrated under non-catalytic conditions, employing experimental transient data of syngas generation rate and compositions under different temperatures and gasifying agents. The DYCORS and GOMORS were employed as the numerical solvers for finding the global optimum solution of the pre-

exponential factors. The calibrated kinetic models based on both single-objective and multi-objective approaches have been validated by experimental data in four different biomass gasification scenarios. The calibrated kinetic model shows an over 95% decrease in terms of integrated squared error (ISE)-based model mismatch when compared to the original kinetic model.

Key words: Biomass gasification, dynamic modelling, experimental calibration, kinetic model.

1. Introduction

Facing the pressure of growing primary energy demand, worldwide attentions on climate change and renewable energy development have been highlighted. In 2019, the renewable power contributes 41% of the increase in energy demand, which is larger than the fossil fuel (oil, gas, and coal) and nuclear[1]. Biomass, as a carbon-neutral energy source, is widely explored in energy production applications and is considered as a candidate for fossil substitutions in energy production[2]. Gasification, which is a thermochemical process to convert the solid fuels (like biomass) into syngas and biochar, has attracted significant research and commercial interest. The biomass gasification technology, when compared to a plethora of other technologies, has the advantage of more efficient and valuable products and less toxic emissions[3].

Modeling is an important tool for both understanding the nature of various chemical and physical effects in biomass gasification and supporting the optimization of process design. Many modeling studies have been conducted for the biomass gasification, and the models can be classified into three different clusters: (i) equilibrium model, (ii) kinetic model, and (iii) data-driven model. The equilibrium model is based on the assumption of thermochemical equilibrium,

and the equilibrium assumption can be derived by specifying all the chemical reactions and species (named as stoichiometric approach) or minimizing the Gibbs free energy of the whole system (named as non-stoichiometric approach)[5-9]. To precisely predict the biomass gasification product distributions over a finite time horizon, the kinetic model is required. Several biomass gasification kinetic models were developed in Aspen Plus to improve the prediction of steady-state energy performances by involving new kinetic schemes and different empirical correlations[10-11]. First-principles kinetic models were also developed to predict the syngas composition, temperature profile, and biochar productions by combining the fuel-bed model with representative particle model (RPM)[12-13]. However, the accuracy of kinetic model is difficult to achieve, due to the microscopic evolution of particle distributions and complex gas-solid contacting processes are hard to model reliably[14]. In the data-driven modeling approaches, such as artificial neuron network (ANN), large amounts of experimental data are employed to training the model endogenous parameters[15]. However, models based on statistic correlations can hardly contribute to a better understanding of the various chemical and physical effects in biomass gasification processes.

From the state of the art, most of the available models can predict the biomass gasification steady-state behaviors. However, studies focused on process dynamic response, which is important for real-time process operation, are relatively scarce. Boujjat et al. developed a solar biomass gasification model based on chemical equilibrium assumptions to analyze the hydrogen-rich syngas during hybrid autothermal/solar and allothermal operations[16]. Mikulandrić et al. established a dynamic ANN model of co-current fixed-bed biomass gasifier, which is trained by operating data from TU Dresden. The model can predict the syngas composition under changing operating conditions but there is still room to improve the prediction[17]. Suárez-Almeida et al.

developed a dynamic fluidized-bed biomass gasification model to analyze the system during start-up and disturbances in air and fuel loads. The model is based on a quasi-equilibrium approach to keep the compromise between model complexity and prediction capability[18].

In our previous study, a hybrid peripheral fragmentation and shrinking-core (HPFS) model[19] was developed to predict the biochar production, PM emission, and syngas generation of biomass gasification. The objective of this work is to develop a dynamic biomass gasification model based HPFS model for better transient prediction accuracy. The pre-exponential factors of kinetic reactions are trained under non-catalytic conditions, employing experimental transient data under different temperatures and gasifying agents. The contributions of this work are not only a calibrated kinetic model of biomass gasification, which can predict the transient outputs of syngas generation, but also demonstrating a systematic way of training complex thermochemical kinetic models with global surrogate optimization techniques to improve transient prediction accuracy .

2. Model development

2.1. Model description and assumptions

Figure 1 depicts the developed dynamic biomass gasification model. The fixed bed operation conditions are employed as the initial and boundary conditions, which are the inputs of the single particle model. The single particle model is based on the HPFS approach[19]. Specifically, the biomass particle porosity builds up with time due to the thermochemical reactions. When the porosity of biomass particle reaches a critical value, the outer layer of the particle is broken into fragmentations and detached from the particle. The peripheral fragmentation leads to both the particle shrinkage and PM emissions. The main assumptions of the model are given as follows:

1) The gaseous species are assumed to be ideal gas
2) The biomass particles are assumed to be a one-dimensional (radial) porous sphere in a time-dependent domain. The governing equations, including mass, energy and momentum balances, are derived by finite volume approach.
3) The gas phase and solid phase of each finite volume are assumed to have the same temperature and temperature gradient
4) The solid phase is assumed to have constant density
5) There is no pressure difference between the external particle surface and the fixed bed gas phase.
6) The homogeneous reactions take place in the lacunar of porous particle.
7) The heterogeneous reactions, which affects the particle porosity evolution, take place only on the solid-gas interface.
8) The shrinkage of particles is due to the peripherical fragmentation when the porosity reaches a critical value.
9) The PM emissions are assumed to be proportional to the detached fragment, which is represented by the particle volumetric shrinkage.

A two-step biomass pyrolysis model[20] is employed in the HPFS framework, including a primary pyrolysis reaction (Eq. 1) and a tar cracking reaction (Eq.2).

$$Volatile \rightarrow 0.268\,CO + 0.295\,CO_2 + 0.094\,CH_4 + 0.5\,H_2 + 0.255\,H_2O + 0.2\,Primary\ tar \quad (1)$$

$$Primary\ tar \rightarrow 0.397\,Secondary\ tar + 2.6\,CO + 0.441\,CO_2 + 0.983\,CH_4 + 2.161\,H_2 \quad (2)$$

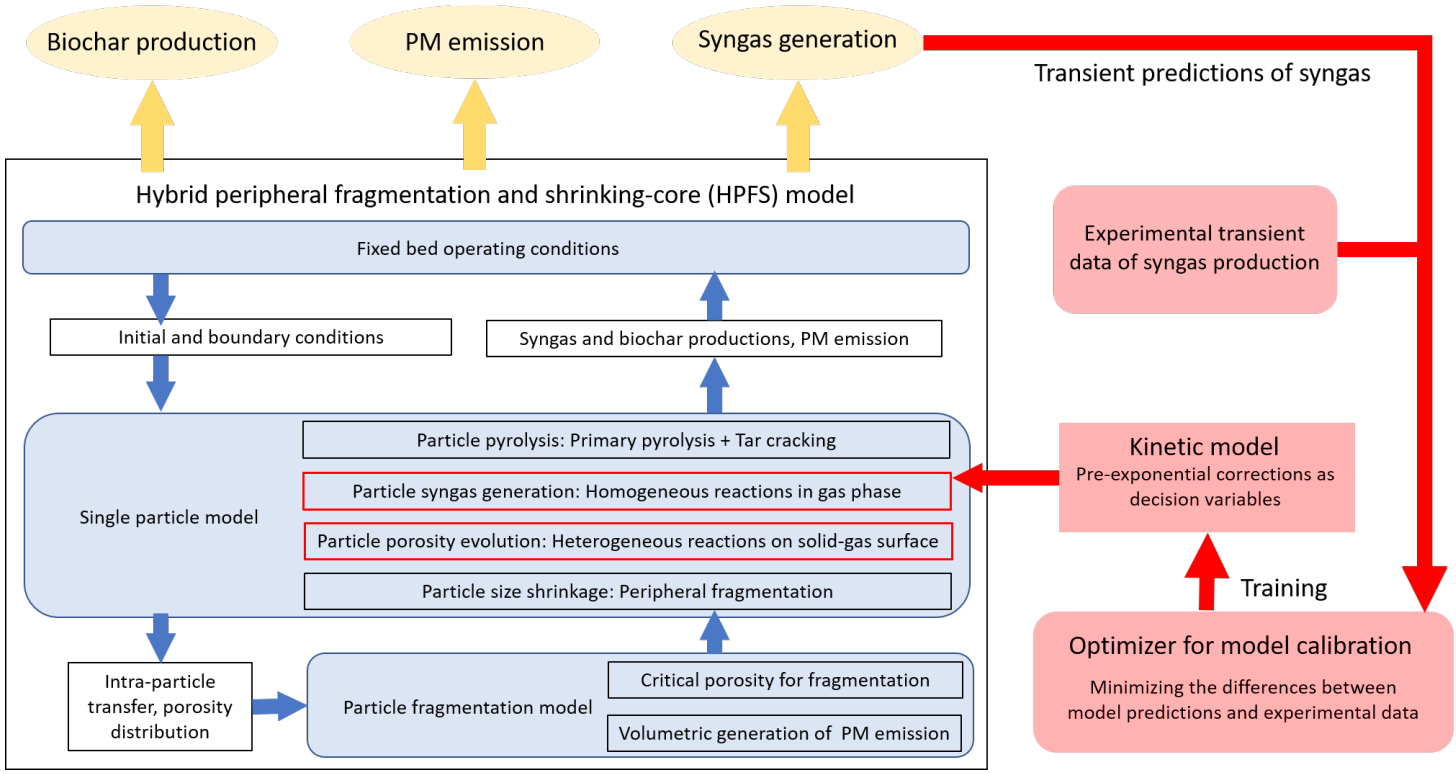

Figure 1. Schematic of the developed dynamic biomass gasification model.

The solid-phase reaction rate is determined based on the film mass-transfer diffusion[20] and the following 5 heterogeneous reactions are considered to take place on the solid-gas interface:

RS1: $2C+O_2 \rightarrow 2CO$

RS2: $2C+O_2 \rightarrow CO_2$

RS3: $C+H_2O \rightarrow CO+H_2$ (3)

RS4: $C+CO_2 \rightarrow 2CO$

RS5: $C+2H_2 \rightarrow CH_4$

The gaseous species are determined based on the turbulent mixing rate using Eddy Dissipation Model[20] and the following 7 homogeneous reactions in the interstitial gas phase of porous biomass particles are employed:

RG1: $PrimaryTar+O_2 \rightarrow H_2O+CO$

RG2: $SecondaryTar+O_2 \rightarrow H_2O+CO$

RG3: $H_2+0.5O_2 \rightarrow H_2O$

RG4: $CO+0.5O_2 \rightarrow CO_2$ (4)

RG5: $H_2O+CO \rightarrow H_2+CO_2$

RG6: $CH_4+1.5O_2 \rightarrow CO+2H_2O$

RG7: $CH_4+H_2O \rightarrow 3H_2+CO$

The governing equations (mass, momentum, and energy balance) and boundary conditions of the HPFS model are addressed in the Supplementary Materials. Refer to the HPFS modeling paper[19] for more model formulation details, including the non-dimensionalization, PDE derivation in MATLAB, and PM emission model formulation.

2.2. Kinetic model calibration

The kinetic reaction rates of the reactions[19] are derived based on literature data, which are shown in Tables 1 and 2. The kinetic reactions rates of RS1, RS3, RS4, RS5 are derived based on Eyring equation (i.e., $k = ATexp\left(\frac{-E}{RT}\right)$), and the kinetic reaction rates of RS2, RG1-7 are formulated based on Arrhenius equation (i.e., $k = Aexp\left(\frac{-E}{RT}\right)$). However, as shown in Figure 2, although the steady-state syngas outputs (accumulated over 30 min time horizon) were in good consistency with the experimental data[19], the accuracy of the syngas transient predictions was not satisfactory. In this work, as depicted in Figure 1, the experimental transient data of syngas generation rate and compositions are employed for training the kinetics of single particle model to improve the transient prediction accuracy. Without change the activation energy term *E*, the pre-exponential factor *A* of kinetic reaction rates are calibrated by addressing pre-exponential correction terms as the following equations:

$$\hat{k} = \alpha ATexp\left(\frac{-E}{RT}\right) \text{for RS1, RS3, RS4, RS5} \quad (5)$$

$$\hat{k} = \alpha Aexp\left(\frac{-E}{RT}\right) \text{for RS2, RG1-7} \quad (6)$$

in which α represents the pre-exponential correction terms. Then, the updated kinetic reaction rates $\hat{r}_i$ are:

$$\hat{r}_i = \alpha_i \cdot r_i \quad (7)$$

in which *i* refers to the reaction index (RS1-5, RG1-7).

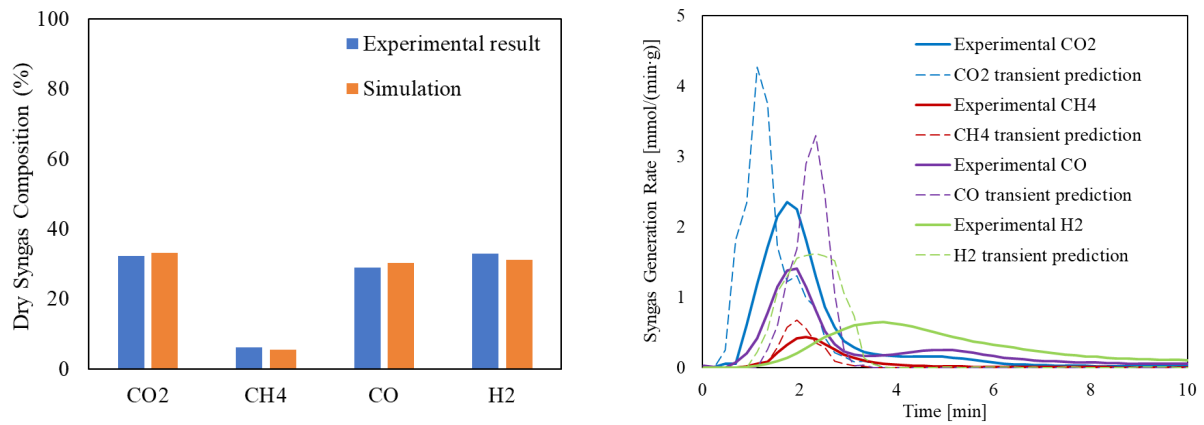

(a) (b)

Figure 2. Experimental validation of dry syngas composition under 600 °C with Ar gasifying agent. (a) accumulated steady-state validation[19]. (b). transient validation.

Table 1. Kinetics of heterogeneous reactions.

Heterogeneous reactions	Kinetic reaction rate [m s^{-1}]	Ref.
RS1	$r_{s1}=2.3T_s\exp\left(\frac{-11100}{T_s}\right)$	[21]
RS2	$\frac{r_{s1}}{r_{s2}}=2512\exp\left(\frac{-6420}{T_g}\right)$	[22]
RS3	$r_{s3}=5.714T_s\exp\left(\frac{-15600}{T_s}\right)$	[23]
RS4	$r_{s4}=589T_s\exp\left(\frac{-26800}{T_s}\right)$	[24]

RS5	$r_{s5}=3.42\times10^{-3}T_s\exp\left(\frac{-15600}{T_s}\right)$	[25]

Table 2. Kinetics of homogeneous reactions.

Heterogeneous reactions	Kinetic reaction rate [kmol $m^{-3}s^{-1}$]	Ref.
RG1	$r_{g1}=1899T_g\exp\left(\frac{-12200}{T_g}\right)C_{PrimaryTar}^{0.5}C_{O_2}\varepsilon$	[24]
RG2	$r_{g2}=1899T_g\exp\left(\frac{-12200}{T_g}\right)C_{SecondaryTar}^{0.5}C_{O_2}\varepsilon$	[24]
RG3	$r_{g3}=3.53\times10^{8.4}\exp\left(\frac{-3670}{T_g}\right)C_{H_2}^{1.1}C_{O_2}^{1.1}\varepsilon$	[26]
RG4	$r_{g4}=1.3\times10^{11}\exp\left(\frac{-15105}{T_g}\right)C_{CO}C_{H_2O}^{0.5}C_{O_2}^{0.5}\varepsilon$	[27]
RG5	$r_{g5}=2.78\exp\left(\frac{-1511}{T_g}\right)\left[C_{CO}C_{H_2O}-\frac{\exp\left(\frac{-7914}{T_g}\right)C_{CO_2}C_{H_2}}{0.0265}\right]$	[28]
RG6	$r_{g6}=1.0\times10^{11.7}\exp\left(\frac{-24357}{T_g}\right)C_{CH_4}^{0.7}C_{O_2}^{0.8}\varepsilon$	[29]
RG7	$r_{g7}=3.0\times10^{8}\exp\left(\frac{-15083}{T_g}\right)C_{CH_4}C_{H_2O}\varepsilon$	[30]

2.2.1. Formulation of kinetic model calibration

The kinetic model calibration is based on solving the optimization problem over the pre-exponential correction α to minimizing the difference between the predicted syngas transient results and the experimental syngas transient data (i.e. model mismatch). The general formulation of the optimization problem for the kinetic model calibration, which is based on integrated squared error (ISE) approach, is given as follows:

$$\begin{aligned} &min\, f(\alpha) = \left\| \sum_{t} \sum_{j} \left(y_{j,t} - \overline{y_{j,t}} \right)^2 \right\|_2 \\ &s.t. \, \alpha = \left[\alpha_{RS1}, \ldots, \alpha_{RS5}, \alpha_{RG1}, \ldots, \alpha_{RG7} \right] > 0 \end{aligned} \tag{8}$$

in which $\overline{y}$ represents the model transient predictions, y represents the experimental transient data, t represents the time horizon, and j represents the transient index. The exponential correction α in Eq. 8 is the decision variable of the optimization problem, which subscripts refer to the kinetic reaction index shown in Tables 1 and 2. In this work, the time horizon t is set from 0 to 30 min, and the transient index j includes the four dry syngas composition (i.e., H_2, CO, CH_4, CO_2) and total dry syngas generation rate.

The calibration is first derived as a single objective optimization problem, employing the experimental transient data on a specific operating condition. The optimization problem is formulated to minimize the model transient mismatch as follows:

$$min\, f_{T,Ag}(\alpha_{T,Ag}) = \left\| \sum_{t} \sum_{j} \left(y_{j,t,T,Ag} - \overline{y_{j,t,T,Ag}} \right)^2 \right\|_2 \tag{9}$$

$$s.t.\alpha_{T,Ag}=\left[\alpha_{RS1},\ldots,\alpha_{RS5},\alpha_{RG1},\ldots,\alpha_{RG7}\right]_{T,Ag}>0$$

in which the two operating condition parameters T and Ag represent the specific gasification temperature and gasifying agent, respectively.

Furthermore, the calibration based on a multi-objective optimization problem is formulated, employing the experimental transient data on multiple operating conditions (different gasification temperatures in this work). The multi-objective problem is derived as follows:

$$\begin{aligned}
&min\, f_{Ag}(\alpha_{Ag})=f_{T_1,Ag}(\alpha_{Ag}),f_{T_2,Ag}(\alpha_{Ag}),\ldots,f_{T_n,Ag}(\alpha_{Ag})\\
&\text{where} f_{T_k,Ag}(\alpha_{Ag})=\left\|\sum_t\sum_j\left(y_{j,t,T_k,Ag}-\overline{y_{j,t,T_k,Ag}}\right)^2\right\|_2,k=1,\ldots,n \qquad (10)\\
&s.t.\alpha_{Ag}=\left[\alpha_{RS1},\ldots,\alpha_{RS5},\alpha_{RG1},\ldots,\alpha_{RG7}\right]_{Ag}>0
\end{aligned}$$

in which T_k represents the different objectives associated with the gasification temperatures.

2.2.2. Numerical solver for model calibration optimization problems

The numerical solver for the single-objective optimization problem in Eq. 9 employs the DYCORS (Dynamic Coordinate search using Response surface model) algorithm[31], which incorporates the idea of dynamically dimensioned search (DDS) algorithm for solving computationally expensive optimization problems. The DYCORS algorithm uses the local metric stochastic radial basis function (LMSRBF) to build surrogate models. Two criteria are considered in selection of the next iterate from random points (generated about the best previous solution): the point's distance from previous evaluated points and the corresponding surrogate model value. A weighted score combining the two criteria is employed to favor a lower surrogate approximation value and a larger minimum distance from previous points. By cycling the

weighted score through a predefined set, the global search and local converge are balanced. DYCORS code can be obtained from PYSOT in Github or from the authors[32].

The main advantage of the DYCORS-LMSRBF algorithm against other nonlinear optimization solvers is the capability to find the global optimum of an expensive problem with relatively few objective function evaluations Here the objective function is the developed gasification model, which is a first-principles model. Unfortunately, the analytical derivatives between the operating conditions and the syngas generation outputs are not available, as the kinetic model is highly compacted with other governing equations over the finite volume of biomass particle. In addition there is no reason to think the model is unimodal so a global optimization method is necessary. Hence, a global optimization algorithm is need that handle the whole gasification model as a black-box function for objective evaluations.

Evolutionary algorithms are not suitable for this problem. The HPFS model is a very computationally expensive model since the average computational time (simulating the 30 min experimental operations) is 254 min, over 4 hours for one evaluation. This is a big challenge for the evolutionary algorithm or genetic algorithm, which typically requires thousands of function evaluations to reach a satisfactory optimal solution.

In the DYCORS-LMSRBF algorithm, most of the trial points generated are evaluated by the RBF interpolation (surrogate model) of the true model, in under a second and only a small fraction of the trial points are used for expensive true objective function evaluations based on HPFS model. Hence the surrogate, which is updated and improved in each iteration is helping to guide efficiently the optimization search.

For the calibration problem based on multi-objective optimization formulation in Eq.10, the numerical solver is derived based on the GOMORS (Gap Optimized Multi-objective

Optimization using Response Surfaces)[33] framework, which is a parallel response surface-assisted algorithm approach to multi-objective optimization. Similar to DYCORS, the GOMORS uses RBF-based surrogate model to compute the approximation of the expensive problem iteratively. In this algorithm, the solutions of single-objective calibration problems are employed in the multi-objective framework as evaluated points of expensive objectives and a subset of current best solutions. The optimization result of the multi-objective problem is a non-dominated best solution set (Pareto set). In the post-Pareto analysis, the solution with minimum sum of all ISE-based model mismatches is proposed as the optimal solution of the calibration problem. The code for GOMORS can be obtained from PYSOT in Github[32]

2.3. Experimental setup

The biomass feedstock used in this study was wood chips, sourced from Ezhou, Hubei Province, China in the 2018 autumn. The fresh wood chips were crushing, sieving, and drying to get the moisture-free fine powders with the particle size of less than 1mm. The densification of raw biomass powders was carried out in a universal material test unit (CMT5205, MTS, China) to form the cylindrical pellets with a diameter of 10 mm and a height of 10 mm. The detailed densification procedure was described in the previous papers[34-35]. The air-dried pellets were used for the following gasification experiments. The detailed densification conditions and properties of air-dried biomass pellet particles are listed in Table 3.

Table 3. Densification conditions and properties of biomass pellet particle.

Densification conditions	
Mass of biomass mixture (g)	0.402 ± 0.003
Water addition for densification (wt%)	10
Holding time for densification (min)	5

Designed size for cylindrical pellet		Diameter: 10 mm; Height: 10 mm	
Designed bulk density (kg/m^3)		1000	
Actual size for cylindrical pellet after air drying		Diameter: 10.35 ± 0.06 mm; Height: 11.04 ± 0.10 mm	
Actual bulk density after air drying (kg/m^3)		842± 3	
Ultimate analysis after air drying (wt%)			
C (ad)	H (ad)	N (ad)	S (ad)
43.18	5.51	1.29	<0.50
Approximate analysis after air drying (wt%)			
Moisture (ad)	Volatile (d)	Fixed carbon (d)	Ash (d)
11.29	76.79	17.30	5.91

The gasification of biomass pellets was conducted in a tubular fixed-bed reaction system (Fig. 4), which contains four parts, namely gas supply and control unit, gasification unit, tar adsorption and cooling unit, and online gas detection unit. In this study, two gasification agents were used: Ar (100 mL/min) and Ar (79 mL/min)/O_2 (21 mL/min). The gasification temperature was varied from 600 to 900 ^oC with a step of 100 ^oC. For each run, a single pellet particle was first placed into the quartz tube (inner diameter of 23 mm and height of 550 mm) and purging with Ar (100 mL/min) for enough time outside of the furnace. After heating the furnace to the target temperature, the supplied gas was switched to the gasification agent for pre-mixing with a time of 15 min. Then the quartz tube was placed into the high-temperature furnace for gasification. After gasification, the produced gases were adsorbed by degreasing cotton and condensed by ice-water, then it was purged into the mass spectrometer (MS) (QGA HPR-20, Hiden Analytical, UK) for online detection. The detailed calibration and setting of MS were described in elsewhere[36-37].

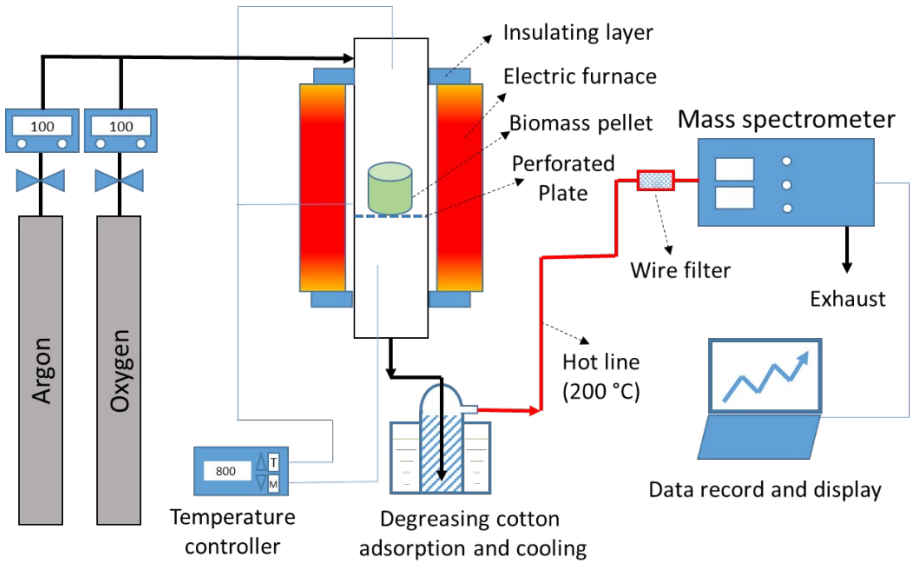

Figure 3. A schematic diagram of the lab-scale gasifier with online recording of the transient concentration of syngas.

3. Result and discussion

3.1. Experimental syngas transient data under different gasification conditions

The experimental transient data of dry syngas production rates and compositions are shown in Figures 4 and 5. The experimental syngas composition data includes the four major syngas components: H_2, CO, CH_4, and CO. The H_2O was not included in the experimental syngas composition data due to part of the water vapor was condensed in the degreasing cotton adsorption and cooling unit, which was designed for tar removal before the gas analyzer.

Figure 4a shows the syngas transient data under Ar gasifying agent with 600 ^oC gasification temperatures. The dry syngas generation rate has a peak tailing type of transient profile with a peak maximum of 2.84 mmol/min per gram biomass. CO_2 is the major component of dry syngas during the peak front (60 to 210 s), and the share of CO increases due to the heterogeneous reactions with the fixed carbon of biomass. The shares of CH_4 and H_2 increases during the peak

tail (210 to 1800 s), and H_2 becomes the major syngas component after 510 s. The syngas transient profile in the 700 °C scenario (shown in Figure 4b) has the similar peak tailing pattern of 600 °C, while a shoulder peak can be found in the 800 °C and 900 °C scenarios (shown in Figures 4c and 4d). When the gasification temperature increase, the peak maximum value of the dry syngas generation rate increase and the time of peak maximum decreases. The heterogeneous reaction RS1 ($2C+O_2 \rightarrow 2CO$) becomes more active in the 800 and 900 °C scenarios during the peak tail, resulted in an increased share of CO and a decreased share of CO_2 when compared to the 600 °C scenario. Note that the dry syngas generation rate is zero during the first 60 seconds in the 600 °C scenario and the duration time of zero dry syngas generation decreases when the gasification temperature increases. This is because only the vaporization of the moisture content generates gases during the start-up of gasification and the H_2O content is not included in the experimental syngas transient data.

Figure 5 shows the syngas transient data under Ar/O_2 gasifying agent with different gasification temperatures. As addressed in subsection 2.3, the Ar/O_2 gasifying agent simulates the air by replacing N_2 with Ar, which can avoid the uncertainty between N_2 and CO in the mass spectrometer. The syngas transient data of Ar/O_2 in the 600 °C is presented in Figure 5a, which has a peak (60 to 350 s) and a flat step (350 to 1100 s). The peak is due to the fast pyrolysis of the biomass volatile content, and the flat step is due to the combustion of the biomass fixed carbon content. CO_2 is the major component of the dry syngas, which has an over 90% share during the flat step. The peak maximum value of the dry syngas generation rate is 2.84 mmol/min per gram biomass in the 600 °C scenarios. The syngas transient profiles in the 700 °C and 800 °C scenario (shown in Figures 5b and 5c) have the similar pattern of the 600 °C profile, while a flat step with higher value and shorter duration time can be found in the 900 °C scenario

(shown in Figure 5d). Note that the increase of CO content after the flat step does not represent a large increase of the transient CO generation rate, as the total dry syngas generation rate drops close to zero. The raise of the CO percentage is mainly due to less CO_2 is generated from the fixed carbon combustion.

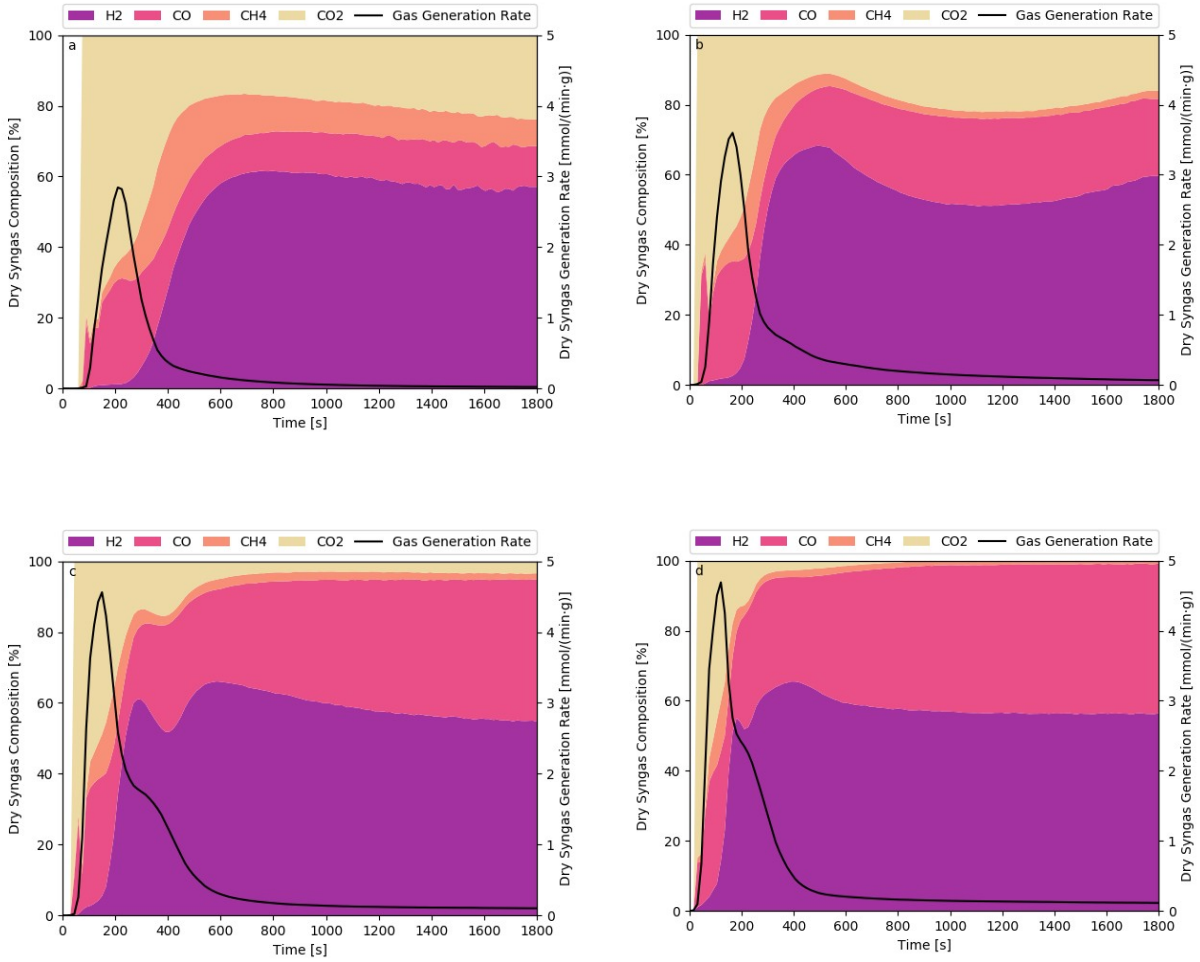

Figure 4. Experimental syngas transient data under Ar gasifying agent. (a) gasification temperature of 600 ºC. (b) gasification temperature of 700 ºC. (c) gasification temperature of 800 ºC. (d) gasification temperature of 900 ºC.

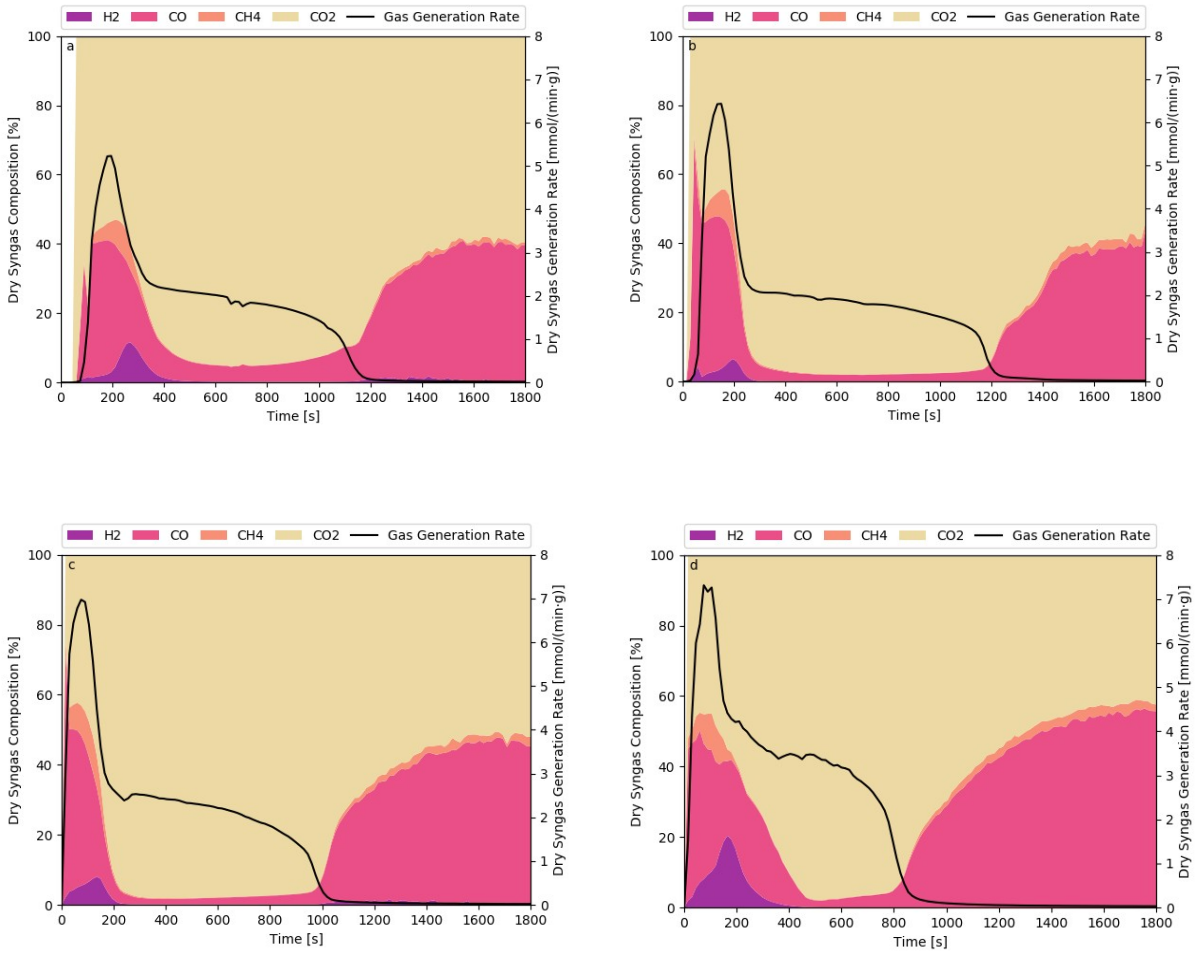

Figure 5. Experimental syngas transient data under Ar/O_2 gasifying agent. (a) gasification temperature of 600 ºC. (b) gasification temperature of 700 ºC. (c) gasification temperature of 800 ºC. (d) gasification temperature of 900 ºC.

3.2. Kinetic model calibration results

In this subsection, the results of 4 case studies associated with the calibrated kinetic model for the syngas transient prediction are presented. The first two scenarios consider the biomass gasification under 600 ºC (Case 1) and 900 ºC (Case 2) with Ar gasifying agent. Figure 6 depicts the syngas transient predictions of three different calibrated kinetic models in Case 1. The first calibrated model (*Ar_600*, shown in Figure 6b) is based on the single objective optimization

employing experimental transient data of 600 °C and Ar gasifying agent, which is similar to the experimental result in Figure 6a. The second kinetic model (*Ar_900*, shown in Figure 6c) is calibrated by a single-objective approach with experimental transient data of 900 °C and Ar gasifying agent. The third model (*Multi-objective*, shown in Figure 6d) is based on multi-objective optimization employing 4 groups of experimental transient data: 600 °C under Ar gasifying agent, 900 °C under Ar gasifying agent, 600 °C under Ar/O_2 gasifying agent, and 900 °C under Ar/O_2 gasifying agent. All the three calibrated model show good consistency with the experimental transient data, and the maximum dry syngas generation rate deviations of the three calibration models are 0.243, 0.971, and 0.602 mmol/min per gram biomass, respectively. The *Ar_600* model shows better performance in Case 1 when compared with *Ar_900*, which is due to the pre-exponential correction terms of *ar_*900 are calibration by experimental transient data under a different operating condition (900 °C and Ar gasifying agent).

Figure 7 depicts the syngas transient predictions of three different calibrated kinetic models in Case 2. Similar to Case 1, the syngas transient predictions of *Ar_600*, *Ar_900*, and *Multi-objective* are shown in Figures 7b, 7c, and 7d, respectively. In Case 2, the *ar_900* model shows better performance when compared with *ar_600*. The maximum dry syngas generation rate deviations of the three calibration models in Case 2 are 0.710, 0.689, and 0.922 mmol/min per gram biomass, respectively. The pre-exponential correction terms and ISE-based model mismatch of the three calibrated models are shown in Tables 4 and 5. Noted that the maximum ISE result of the three calibrated models is 12.48 in Case 1, which has an over 95% decrease when compared to the original transient mismatch shown in Figure 2b (ISE result of 214.35 over the 30 min horizon).

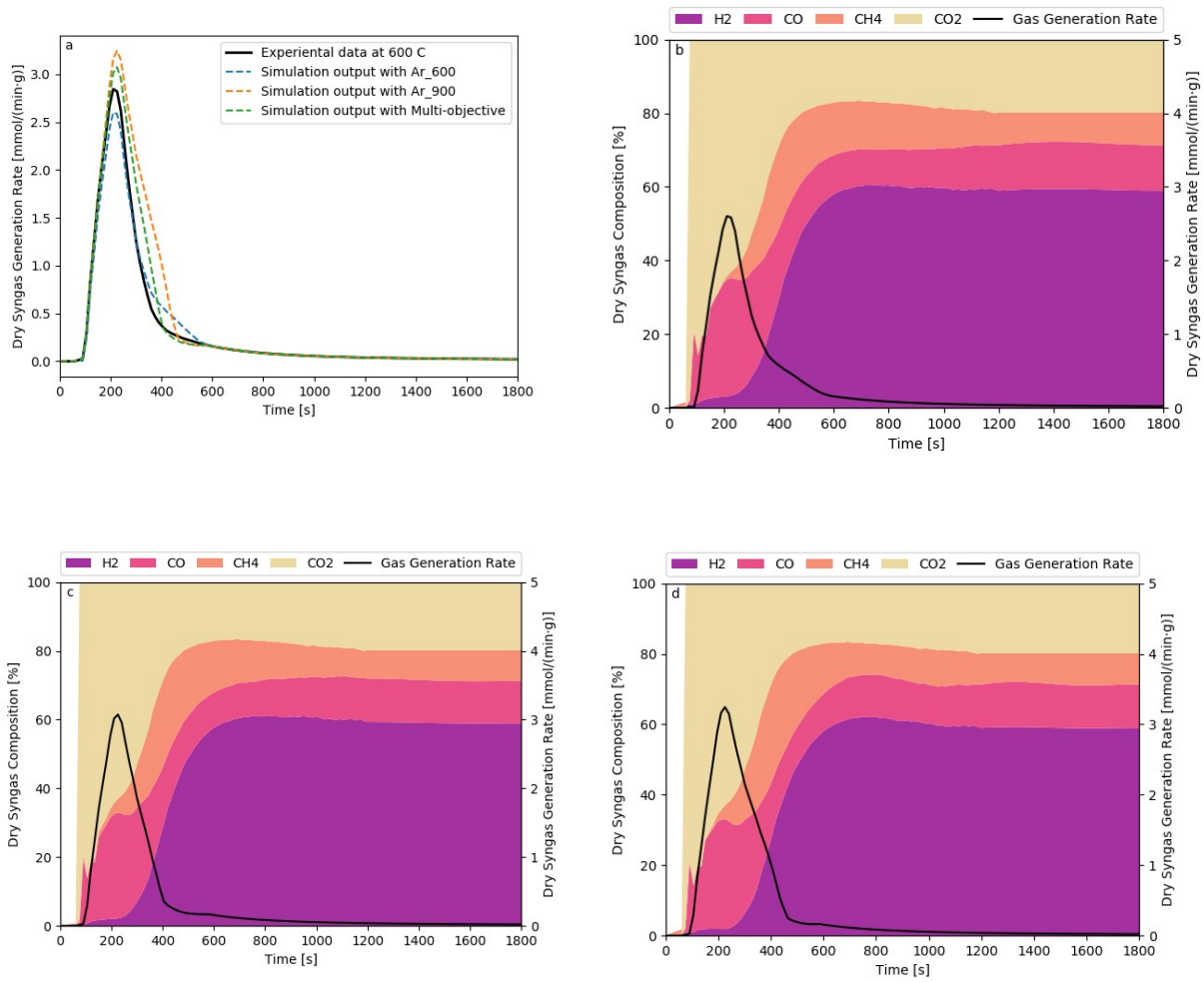

Figure 6. Case 1: syngas transient calibration results under 600 ºC with Ar gasifying agent. (a). overall all syngas generation rates employing different kinetic models. (b). syngas transient employing kinetic model optimized at 600 ºC. (c). syngas transient employing kinetic model optimized at 900 ºC. (d). syngas transient employing kinetic model of multi-objective optimization.

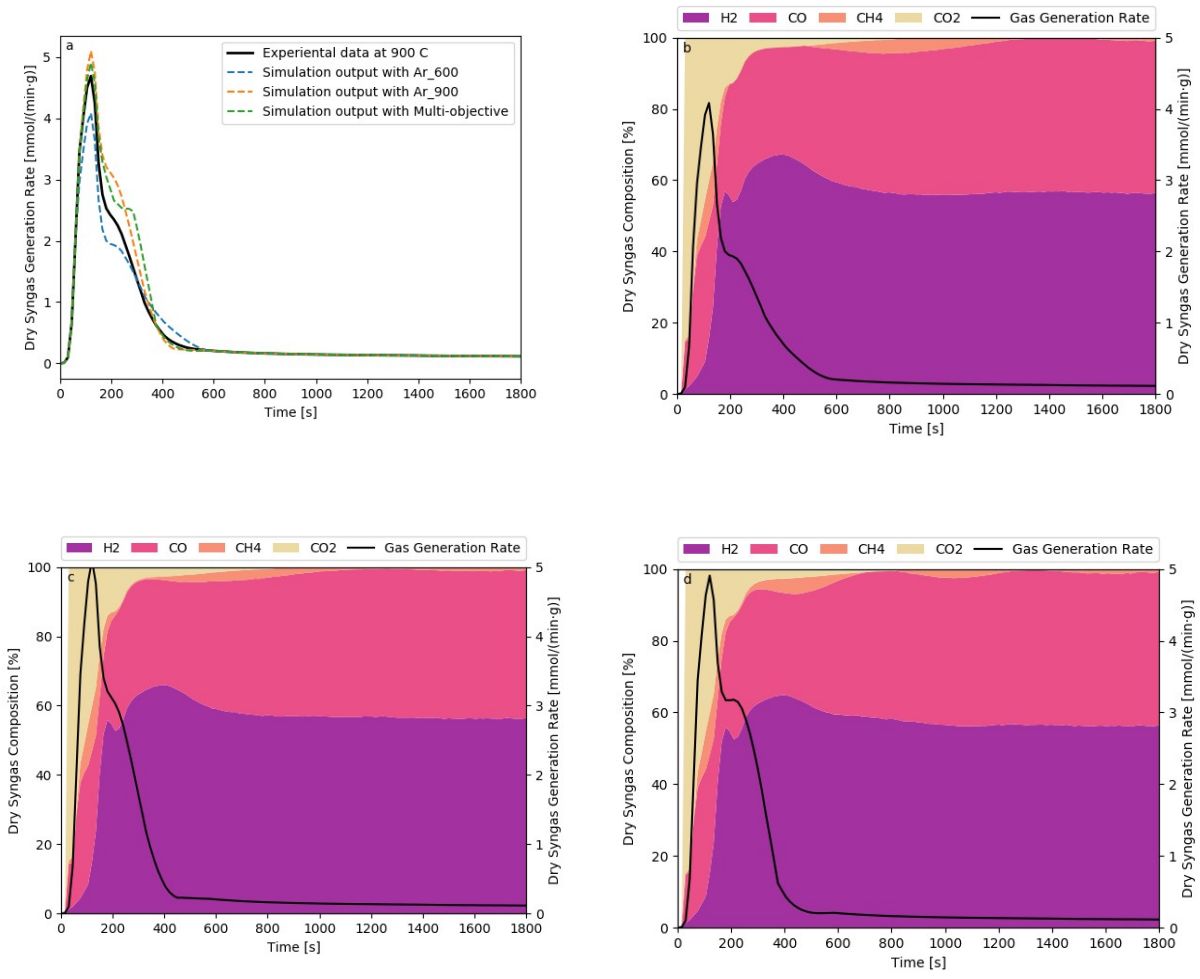

Figure 7. Case 2: syngas transient calibration results under 900 ºC with Ar gasifying agent. (a). overall all syngas generation rates employing different kinetic models. (b). syngas transient employing kinetic model optimized at 600 ºC. (c). syngas transient employing kinetic model optimized at 900 ºC. (d). syngas transient employing kinetic model of multi-objective optimization.

Table 4. Pre-exponential correction terms of *Ar_600*, *Ar_900*, and *Multi-objective* models

	Ar_600	*Ar_900*	*Multi-objective*

α_{RS1}	0.99	1	1
α_{RS2}	1	0.99	0.99
α_{RS3}	2.15×10^{-2}	3.95×10^{-2}	2.57×10^{-2}
α_{RS4}	32.6	3.82	8.21
α_{RS5}	5.74×10^{3}	1.17×10^{2}	6.85×10^{2}
α_{RG1}	1.68	7.54	5.22
α_{RG2}	0.98	2.15	1.49
α_{RG3}	7.91	6.2×10^{3}	4.7×10^{3}
α_{RG4}	0.49	9.05	2.17
α_{RG5}	9.74×10^{2}	3.74×10^{3}	2.11×10^{3}
α_{RG6}	6.12	8.44	6.26
α_{RG7}	3.83×10^{-2}	0.57	0.17

Table 5. ISE-based model mismatches of *Ar_600*, *Ar_900*, and *Multi-objective* models

ISE analysis result	*Ar_600*	*Ar_900*	*Multi-objective*
Case 1	4.75	12.48	7.85

Case 2	17.26	8.22	10.74

The Cases 3 and 4 consider the biomass gasification under 600 ^{o}C and 900 ^{o}C with Ar/O_2 (air) gasifying agent, respectively. Figure 8 depicts the syngas transient predictions of three calibrated kinetic models in Case 3. The *Ar/O_2_600* and *Ar/O_2_900* models are based on the single objective approach employing experimental transient data of 600 ^{o}C and 900 ^{o}C under Ar/O_2 gasifying agent, respectively. The *Multi-objective* model, as shown in Figure 8d, is the same calibrated model used in Cases 1 and 2. The maximum dry syngas generation rate deviations of the three calibration models are 1.161, 0.448, and 0.823 mmol/min per gram biomass, respectively. Similar to Case 1, the *Ar/O_2_600* model shows better performance in Case 3 when compared with *Ar/O_2_900*.

Figures 9 depicts the syngas transient predictions of three different calibrated kinetic models in Case 4. The syngas transient predictions of *Ar/O_2_600*, *Ar/O_2_900*, and *Multi-objective* models are shown in Figures 9b, 9c, and 9d, respectively. In Case 4, the *air_900* model shows better performance when compared with *Ar/O_2_600*. The maximum dry syngas generation rate deviations of the three calibration models in Case 4 are 0.401, 1.341, and 0.859 mmol/min per gram biomass, respectively. The pre-exponential correction terms and ISE-based model mismatch of the three calibrated models are shown in Tables 6 and 7. The *Multi-objective* model shows satisfactory robustness for predicting syngas transient responses in all four gasification scenarios.

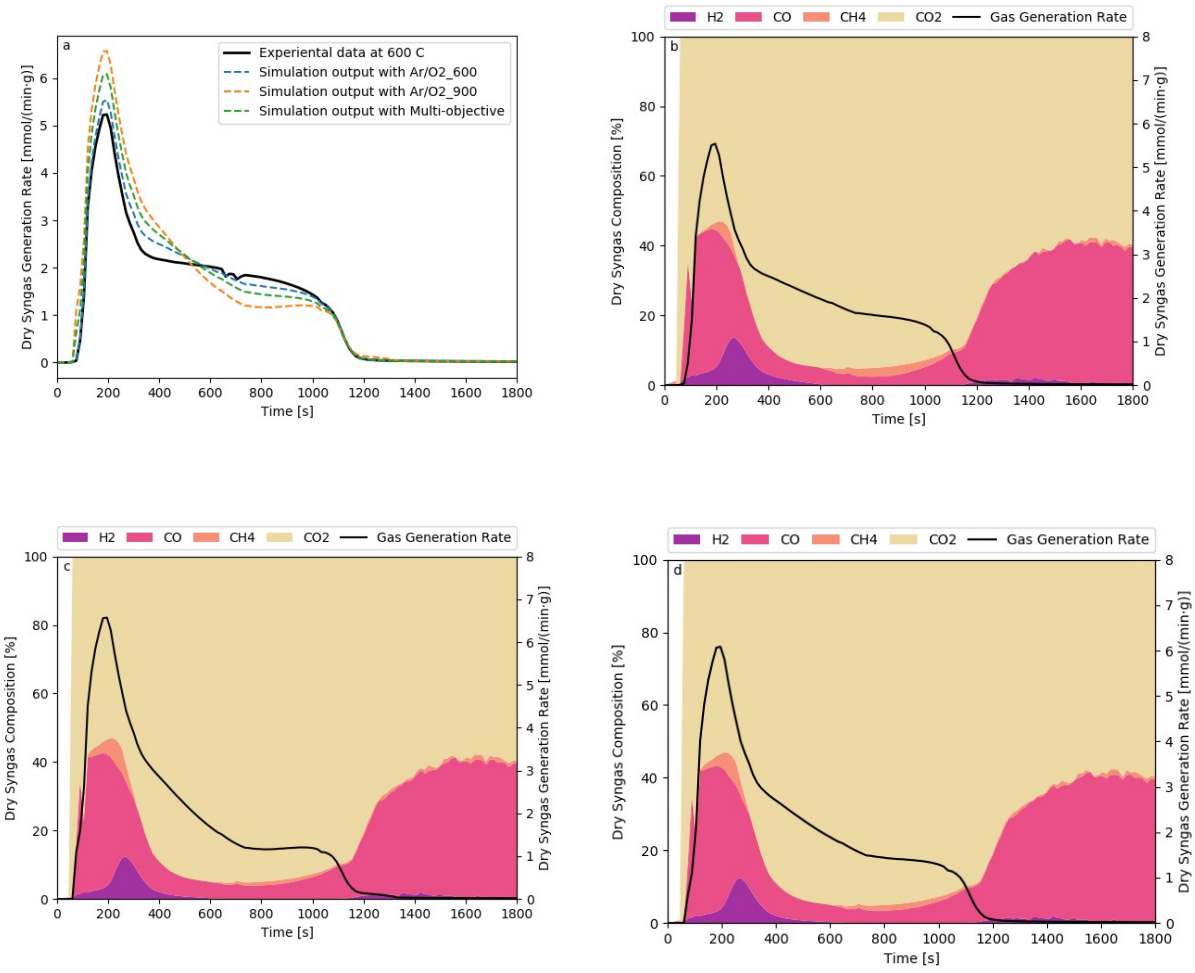

Figure 8. Case 3: syngas transient calibration results under 600 ºC with Ar/O_2 gasifying agent. (a). overall all syngas generation rate employing different kinetic kinetic models. (b). syngas transient employing kinetic model optimized at 600 ºC, (c). syngas transient employing kinetic model optimized at 900 ºC, (d). syngas transient employing kinetic model of multi-objective optimization.

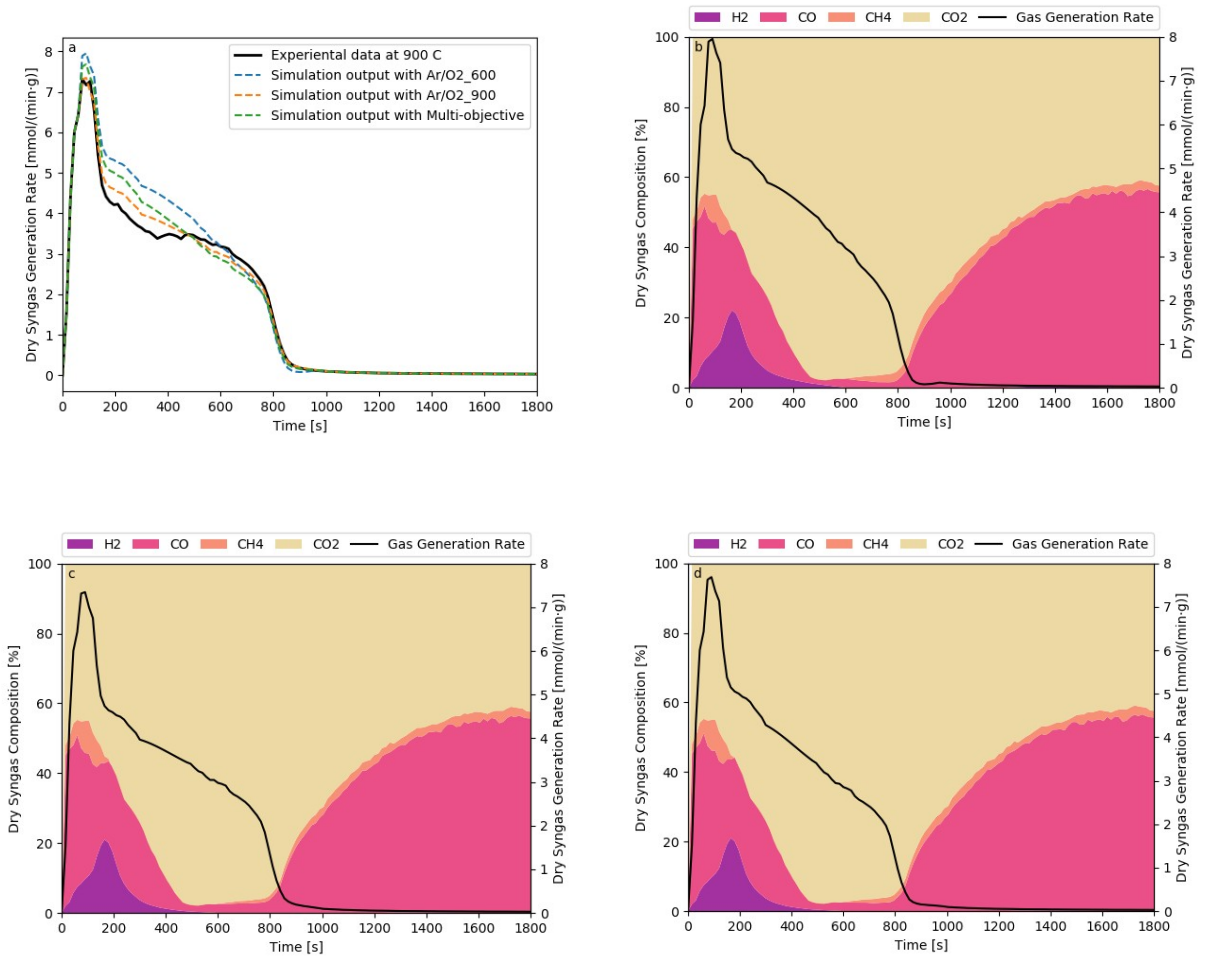

Figure 9. Case 4: syngas transient calibration results under 900 ºC with Ar/O_2 gasifying agent. (a). overall all syngas generation rate employing different kinetic kinetic models. (b). syngas transient employing kinetic model optimized at 600 ºC, (c). syngas transient employing kinetic model optimized at 900 ºC, (d). syngas transient employing kinetic model of multi-objective optimization.

Table 6. Pre-exponential correction terms of *Ar/O_2_600*, *Ar/O_2_900*, and *Multi-objective* models

	Ar/O_2_600	*Ar/O_2_900*	*Multi-objective*

α_{RS1}	0.99	1	1
α_{RS2}	1	0.99	0.99
α_{RS3}	2.05×10^{-2}	5.22×10^{-2}	2.57×10^{-2}
α_{RS4}	17.4	2.96	8.21
α_{RS5}	5.11×10^{3}	62.5	6.85×10^{2}
α_{RG1}	4.91	10.35	5.22
α_{RG2}	0.98	2.19	1.49
α_{RG3}	6.75	9.88×10^{3}	4.7×10^{3}
α_{RG4}	0.23	3.05	2.17
α_{RG5}	1.64×10^{3}	1.74×10^{4}	2.11×10^{3}
α_{RG6}	1.72	25.3	6.26
α_{RG7}	9.89×10^{-3}	0.18	0.17

Table 7. ISE-based model mismatch of *Ar/O₂_600*, *Ar/O₂_900*, and *Multi-objective* models

ISE analysis result	*Ar/O₂_600*	*Ar/O₂_900*	*Multi-objective*
Case 3	14.28	50.04	27.51

Case 4	60.36	22.24	36.18

Conclusions

In this work, the kinetic model based on literature data was trained by optimizing the pre-exponential correction terms of both homogeneous and heterogeneous reactions. The calibrated kinetic models based on both single-objective and multi-objective global surrogate optimization with DYCORS and GOMORS approaches successfully predict the experimental syngas generation transient responses in four different biomass gasification scenarios, and have an over 95% decrease in terms of ISE-based transient mismatch when compared to the original model. The proposed calibration method provides a systematic way of training complex thermochemical kinetic models to improve transient prediction accuracy. The calibrated dynamic biomass gasification model can be further employed for real-time optimization and advanced operation control in the gasification processes.

Acknowledgments

This research is supported by the National Research Foundation (NRF), Prime Minister's Office, Singapore under its Campus for Research Excellence and Technological Enterprise (CREATE) programme (Grant Number R-706-001-102-281). The authors utilized the opensource pySOT package in GitHub for optimization.

Notations

A	pre-exponential factor	-
C	mole concentration	mol m^{-3}
E	activation energy	J mol^{-1}
f	objective function	-
k	reaction rate constant	depends on reaction order
R	gas constant	8.314 J mol^{-1} K^{-1}
r	original reaction rate	mol $m^{-3}s^{-1}$ for RG1-7 mol $m^{-2}s^{-1}$ for RS1-5
$\hat{r}_i$	trained reaction rate	mol $m^{-3}s^{-1}$ for RG1-7 mol $m^{-2}s^{-1}$ for RS1-5
T	temperature	K
y	the experimental data	-
$\overline{y}$	model outputs	-

Greek letters

α	pre-exponential correction factors	-
ε	porosity	-

Subscripts

Ag	gasifying agent index
g	pertains to gas phase
i	pertains to specie or component in gas phase with index i
j	the model output index

k	pertains to reaction number or gasification condition with index k
s	pertains to solid phase
t	transient variables
T	gasification temperature index

References

1. Looney B. Full report–BP statistical review of world energy 2020.

2. You S, Ok YS, Chen SS, Tsang DC, Kwon EE, Lee J, Wang CH. A critical review on sustainable biochar system through gasification: energy and environmental applications. Bioresource technology. 2017;246:242-53.

3. Damartzis T, Zabaniotou A. Thermochemical conversion of biomass to second generation biofuels through integrated process design—A review. Renewable and Sustainable Energy Reviews. 2011;15(1):366-78.

4. Baruah D, Baruah DC. Modeling of biomass gasification: A review. Renewable and Sustainable Energy Reviews. 2014;39:806-15.

5. Zainal ZA, Ali R, Lean CH, Seetharamu KN. Prediction of performance of a downdraft gasifier using equilibrium modeling for different biomass materials. Energy conversion and management. 2001;42(12):1499-515.

6. Melgar A, Pérez JF, Laget H, Horillo A. Thermochemical equilibrium modelling of a gasifying process. Energy conversion and management. 2007;48(1):59-67.

7. Ratnadhariya JK, Channiwala SA. Three zone equilibrium and kinetic free modeling of biomass gasifier–a novel approach. Renewable energy. 2009;34(4):1050-8.

8. Basu P. Biomass gasification and pyrolysis: practical design and theory. Academic press; 2010.

9. Yan WC, Shen Y, You S, Sim SH, Luo ZH, Tong YW, Wang CH. Model-based downdraft biomass gasifier operation and design for synthetic gas production. Journal of cleaner production. 2018;178:476-93.

10. Ahmed AM, Salmiaton A, Choong TS, Azlina WW. Review of kinetic and equilibrium concepts for biomass tar modeling by using Aspen Plus. Renewable and Sustainable Energy Reviews. 2015;52:1623-44.

11. Han J, Liang Y, Hu J, Qin L, Street J, Lu Y, Yu F. Modeling downdraft biomass gasification process by restricting chemical reaction equilibrium with Aspen Plus. Energy conversion and management. 2017;153:641-8.

12. Di Blasi C. Dynamic behaviour of stratified downdraft gasifiers. Chemical engineering science. 2000;55(15):2931-44.

13. Giltrap DL, McKibbin R, Barnes GR. A steady state model of gas-char reactions in a downdraft biomass gasifier. Solar Energy. 2003;74(1):85-91.

14. Safarian S, Unnþórsson R, Richter C. A review of biomass gasification modelling. Renewable and Sustainable Energy Reviews. 2019;110:378-91.

15. Baruah D, Baruah DC, Hazarika MK. Artificial neural network based modeling of biomass gasification in fixed bed downdraft gasifiers. Biomass and Bioenergy. 2017;98:264-71.

16. Boujjat H, Junior GM, Rodat S, Abanades S. Dynamic simulation and control of solar biomass gasification for hydrogen-rich syngas production during allothermal and hybrid solar/autothermal operation. International Journal of Hydrogen Energy. 2020;45(48): 25827-25837.

17. Mikulandrić R, Böhning D, Böhme R, Helsen L, Beckmann M, Lončar D. Dynamic modelling of biomass gasification in a co-current fixed bed gasifier. Energy Conversion and Management. 2016;125:264-76.

18. Suárez-Almeida M, Gómez-Barea A, Ghoniem AF, Nilsson S, Leckner B. Modeling the transient response of a fluidized-bed biomass gasifier. Fuel. 2020:117226.

19. Yao Z, He X, Hu Q, Cheng W, Yang H, Wang CH. A Hybrid Peripheral Fragmentation and Shrinking-core Model for Fixed-bed Biomass Gasification. Chemical Engineering Journal. 2020:124940.

20. Yao Z, You S, Ge T, Wang CH. Biomass gasification for syngas and biochar co-production: Energy application and economic evaluation. Applied Energy. 2018;209:43-55.

21. Hobbs ML, Radulovic PT, Smoot DL. Combustion and gasification of coals in fixed-beds. Progress in Energy and Combustion Science. 1993;19(6):505-86.

22. Arthur JR. Reactions between carbon and oxygen. Transactions of the Faraday Society. 1951;47:164-78.

23. Yoon H, Wei J, Denn MM. A model for moving−bed coal gasification reactors. AIChE Journal. 1978;24(5):885-903.

24. Siminski VJ, Wright FJ, Edelman R, Economos C, Fortune O. Research on Methods of Improving the Combustion Characteristics of Liquid Hydrocarbon Fuels. Volume I.

Experimental Determination of Ignition Delay Times in Subsonic Flow Systems. Volume 2. Kinetics Modeling and Supersonic Testing. ESSO Research and Engineering CO Lindennj Government Research Lab; 1972.

25. Gerber S, Behrendt F, Oevermann M. An Eulerian modeling approach of wood gasification in a bubbling fluidized bed reactor using char as bed material. Fuel. 2010;89(10):2903-17.

26. Varma AK, Chatwani AU, Bracco FV. Studies of premixed laminar hydrogen-air flames using elementary and global kinetics models. Combustion and flame. 1986;64(2):233-6.

27. Howard JB, Williams GC, Fine DH. Kinetics of carbon monoxide oxidation in postflame gases. In Symposium (International) on Combustion 1973; 14(1):975-986).

28. Macak J, Malecha J. Mathematical model for the gasification of coal under pressure. Industrial & Engineering Chemistry Process Design and Development. 1978;17(1):92-8.

29. Dryer FL, Glassman I. High-temperature oxidation of CO and CH4. InSymposium (International) on combustion 1973; 14(1): 987-1003).

30. Jones WP, Lindstedt RP. Global reaction schemes for hydrocarbon combustion. Combustion and flame. 1988;73(3):233-49.

31. Regis RG, Shoemaker CA. Combining radial basis function surrogates and dynamic coordinate search in high-dimensional expensive black-box optimization. Engineering Optimization. 2013;45(5):529-55.

32. Eriksson D, Bindel D, Shoemaker CA. pySOT and POAP: An event-driven asynchronous framework for surrogate optimization. arXiv 2019;1908.00420.

33. Akhtar T, Shoemaker CA. Multi objective optimization of computationally expensive multi-modal functions with RBF surrogates and multi-rule selection. Journal of Global Optimization. 2016;64(1):17-32.

34. Hu Q, Yang H, Xu H, Wu Z, Lim CJ, Bi XT, Chen H. Thermal behavior and reaction kinetics analysis of pyrolysis and subsequent in-situ gasification of torrefied biomass pellets. Energy Conversion and Management. 2018;161:205-14.

35. Hu Q, Shao J, Yang H, Yao D, Wang X, Chen H. Effects of binders on the properties of bio-char pellets. Applied Energy. 2015;157:508-16.

36. Hu Q, Dai Y, Wang CH. Steam co-gasification of horticultural waste and sewage sludge: Product distribution, synergistic analysis and optimization. Bioresource Technology. 2020;301:122780.

37. Hu Q, Wang CH. Insight into the Fe2O3/CaO-based chemical looping process for biomass conversion. Bioresource Technology. 2020:123384.